

Non-Gaussian transverse momentum fluctuations from impact parameter fluctuations

Rupam Samanta,^{1,2} João Paulo Picchetti,³ Matthew Luzum,³ and Jean-Yves Ollitrault²

¹*AGH University of Science and Technology, Faculty of Physics and Applied Computer Science, aleja Mickiewicza 30, 30-059 Cracow, Poland*

²*Université Paris Saclay, CNRS, CEA, Institut de physique théorique, 91191 Gif-sur-Yvette, France*

³*Instituto de Física, Universidade de São Paulo, Rua do Matão, 1371, Butantã, 05508-090, São Paulo, Brazil*

The transverse momentum per particle, $[p_t]$, fluctuates event by event in ultrarelativistic nucleus-nucleus collisions, for a given multiplicity. These fluctuations are small and approximately Gaussian, but a non-zero skewness has been predicted on the basis of hydrodynamic calculations, and seen experimentally. We argue that the mechanism driving the skewness is that, if the system thermalizes, the mean transverse momentum increases with impact parameter for a fixed collision multiplicity. We postulate that fluctuations are Gaussian at fixed impact parameter, and that non-Gaussianities solely result from impact parameter fluctuations. Using recent data on the variance of $[p_t]$ fluctuations, we make quantitative predictions for their skewness and kurtosis as a function of the collision multiplicity. We predict in particular a spectacular increase of the skewness below the knee of the multiplicity distribution, followed by a fast decrease.

There is now wide consensus that collisions between atomic nuclei at ultrarelativistic energies produce a tiny droplet of fluid made of quarks and gluons, which quickly thermalizes as a result of the strong interaction. For two decades, evidence for the formation of a fluid has largely relied on the observation of anisotropic flow, seen through azimuthal correlations between outgoing particles [1]. Evidence of a different nature has recently been revealed [2], based on the fluctuations of the transverse momentum per particle, $[p_t]$, across collision events with the same multiplicity. These are traditional observables of nucleus-nucleus collisions [3–8], which are used to constrain theoretical models [9–12]. The new observation by the ATLAS collaboration is that the variance of these fluctuations in Pb+Pb collisions decreases by a factor ~ 2 over a narrow multiplicity range [13] corresponding to ultracentral collisions [14–21], where $[p_t]$ fluctuations had not yet been analyzed. This decrease is naturally explained by invoking thermalization. Thermalization indeed implies that $[p_t]$ is linked with the density, which depends on impact parameter. The observed decrease then results from the decrease of impact parameter fluctuations in collisions with the largest multiplicity.

In this paper, we show that this mechanism also implies that fluctuations of $[p_t]$ are strongly non-Gaussian in ultracentral collisions.¹ Using the same model of $[p_t]$ fluctuations as in Ref. [2], we make quantitative, parameter-free predictions for the skewness and excess kurtosis, which are standard measures of the non-Gaussianity.

In order to understand the fluctuations of $[p_t]$ at fixed multiplicity N_{ch} , one must take into account two effects. The first is that collision events with the same multiplicity N_{ch} can have different impact parameter b . This

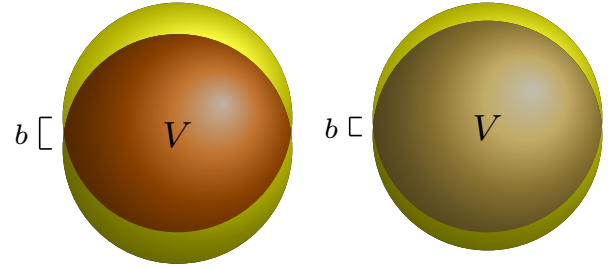


FIG. 1. Representation of Pb+Pb collisions with the same multiplicity and different impact parameters $b = 1.8$ fm (left) and $b = 1.0$ fm (right), corresponding to centrality fractions $c_b \simeq 1.5$ % and $c_b \simeq 0.5$ %. The interval between these two values is the typical spread of c_b for fixed multiplicity. The larger value of b goes along with a smaller collision volume, implying a larger density, symbolically depicted with a darker color.

simple fact is often overlooked because N_{ch} is traditionally used as an estimator of the centrality, as defined by b . The second effect is that for a given multiplicity N_{ch} , $[p_t]$ depends on impact parameter b . Larger b implies a smaller collision volume V (Fig. 1), hence larger density N_{ch}/V . If the system thermalizes, the temperature is higher and the momentum per particle $[p_t]$ is larger.

We first explain the origin of non-Gaussian fluctuations on the basis of a simplified model, where $[p_t]$ is a single-valued function of N_{ch} and b . Instead of b , we use the centrality fraction $c_b \simeq \pi b^2 / \sigma_{Pb}$ [23] (where σ_{Pb} is the inelastic cross section of the Pb+Pb collision) as an equivalent variable throughout this paper. The variation of c_b for fixed N_{ch} is small enough that the dependence of $[p_t]$ on c_b can be linearized:²

$$[p_t] = p_t^{\min} + \lambda c_b, \quad (1)$$

¹ It has already been observed that hydrodynamic calculations imply a significant skewness of $[p_t]$ fluctuations [22], but the crucial role of impact parameter has so far been overlooked.

² Note that observables depend quadratically on b for small b for

where p_t^{\min} and λ depend on N_{ch} .

The probability distribution of $[p_t]$ is then determined by that of c_b . The probability distribution of c_b for fixed N_{ch} , $p(c_b|N_{ch})$, can easily be determined [23]. First, one assumes that the distribution of N_{ch} at fixed impact parameter is Gaussian:

$$p(N_{ch}|c_b) = \frac{1}{\sqrt{2\pi}\sigma_{N_{ch}}(c_b)} \exp\left(-\frac{(N_{ch} - \overline{N_{ch}}(c_b))^2}{2\sigma_{N_{ch}}(c_b)^2}\right). \quad (2)$$

For ultracentral collisions where $c_b \ll 1$, one neglects the dependence of $\sigma_{N_{ch}}$ on c_b , and linearizes the variation of the mean:

$$\overline{N_{ch}}(c_b) = N_{\text{knee}} - \beta c_b, \quad (3)$$

where N_{knee} is the knee, defined as the average multiplicity for $b = 0$, and β determines the decrease of the multiplicity with centrality. The values of these parameters can be obtained by fitting the measured distribution of N_{ch} [23]. In our numerical calculations, we use the values appropriate for Pb+Pb collisions at $\sqrt{s_{NN}} = 5.02$ TeV, and for the charged particle multiplicity seen by the inner detector of ATLAS, namely: $N_{\text{knee}} = 3680$, $\sigma_{N_{ch}} = 168$, $\beta = 18300$ [2].

The probability distribution of c_b for fixed N_{ch} is then given by Bayes' theorem:³

$$p(c_b|N_{ch}) = \frac{p(N_{ch}|c_b)}{p(N_{ch})} \propto \exp\left(-\frac{(N_{ch} - N_{\text{knee}} + \beta c_b)^2}{2\sigma_{N_{ch}}^2}\right), \quad (4)$$

where we have used Eqs. (2) and (3). Eq. (4) shows that the distribution of c_b is Gaussian, with a width $\sigma_{N_{ch}}/\beta \simeq 0.9\%$. It is, however, a *truncated* Gaussian, because of the boundary condition $c_b \geq 0$ [23]. Eq. (1) then implies that the probability distribution of $[p_t]$ is also a truncated Gaussian, with the boundary condition $[p_t] \geq p_t^{\min}$. This is illustrated by the solid curves in Fig. 2, which will be discussed in more detail below.

This truncation has several effects. First, the distribution of $[p_t]$ becomes narrower, resulting in a decrease of the variance. This decrease has been seen by ATLAS [13] and analyzed in Ref. [2]. Second, the truncation generates non-Gaussian features such as skewness and kurtosis, which are the focus of this paper.

We now introduce a more realistic model of $[p_t]$ fluctuations, in order to take into account that $[p_t]$ can vary even if both N_{ch} and c_b are fixed. We assume, following Ref. [2], that the joint distribution of N_{ch} and $[p_t]$ at fixed c_b , $p([p_t], N_{ch}|c_b)$, is a correlated Gaussian. The

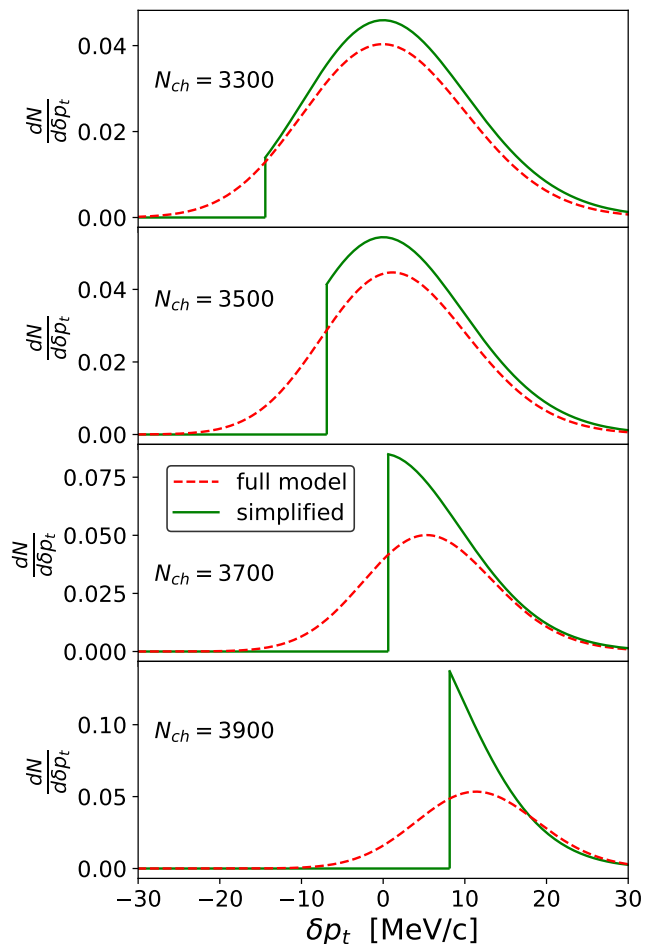


FIG. 2. Probability distribution of $[p_t]$ for various values of the multiplicity N_{ch} . If one defines centrality according to N_{ch} , the centrality fractions corresponding to these values of N_{ch} are, from top to bottom, 2.2%, 1.1%, 0.3% and 0.04%. We decompose $[p_t]$ as $[p_t] = p_{t0} + \delta p_t$, where p_{t0} is a constant, and we only plot the distribution of δp_t . The solid lines correspond to the simplified model where $[p_t]$ only depends on N_{ch} and impact parameter (Eq. (1)). The dashed lines correspond to a more realistic model, assuming Gaussian fluctuations of $[p_t]$ for fixed N_{ch} and c_b .

simplified model above corresponds to the limit where the correlation is maximal and there is a one-to-one correspondence between $[p_t]$ and N_{ch} at fixed c_b .

The Gaussian ansatz can be justified in the following way. In a hydrodynamic model, fluctuations of N_{ch} and $[p_t]$ both stem from fluctuations of the initial density profile. At fixed b , these density fluctuations originate from quantum fluctuations, either in the wave functions of incoming nuclei [25–27] or in the collision dynamics. At ultrarelativistic energies, causality implies that fluctuations in different locations in the transverse plane are independent. Therefore, fluctuations of N_{ch} and $[p_t]$ can be thought of resulting from a large number of independent contributions, and the central limit theorem implies

symmetry reasons [24], which forbids a dependence of the type $\sqrt{c_b}$ for small b .

³ c_b is the cumulative distribution of b , therefore, $p(c_b) = 1$ by construction.

that their fluctuations are approximately Gaussian.

The two-dimensional Gaussian distribution has five parameters: The mean and standard deviation of N_{ch} and of $[p_t]$, and the Pearson correlation coefficient r between N_{ch} and $[p_t]$. All these parameters may depend on c_b . We now explain how they are obtained. We use experimental data when possible, and model calculations otherwise.

From the probability distribution of the charged multiplicity $P(N_{ch})$, which is accurately measured, one can infer the c_b -dependence of the mean multiplicity, $\overline{N_{ch}}(c_b)$, as well as the standard deviation $\sigma_{N_{ch}}$ for $c_b = 0$ [2, 23]. On the other hand, the c_b dependence of $\sigma_{N_{ch}}$ is not at all constrained by existing data. We therefore borrow this information from state-of-the-art models which have been tuned to experiment through Bayesian analyses. We use two models, one by the Duke group [28] and the other by the JETSCAPE collaboration [29]. The JETSCAPE analysis is tuned to a larger set of data, including several collision energies. The Duke analysis is specifically tuned to 5.02 TeV data, which are the ones we use in this paper, and differs from the JETSCAPE analysis in the sense that nucleon substructure is taken into account, which may have an effect on fluctuations. We evaluate $\sigma_{N_{ch}}(c_b)$ for both models, in a way which is explained in detail in App. A. The Duke parametrization predicts that $\sigma_{N_{ch}}$ increases between $b = 0$ and $b = 3.5$ fm, while the JETSCAPE parametrization predicts a slight decrease. We use the difference between these two models as an estimate of the error in our predictions.

The other parameters of our Gaussian model are the mean, p_{t0} , and the standard deviation, σ_{p_t} , of $[p_t]$ at fixed impact parameter, and the Pearson correlation coefficient r between N_{ch} and $[p_t]$. Based on the observation that the variation of the mean value of p_t is below the percent level in the 0-30% centrality range [30], we assume that p_{t0} is independent of impact parameter. We decompose $[p_t] = p_{t0} + \delta p_t$, and we only model the distribution of δp_t , so that our results are independent of p_{t0} . We assume that σ_{p_t} varies with c_b like a power law of the mean multiplicity:

$$\sigma_{p_t}(c_b) = \sigma_{p_t}(0) \left(\frac{N_{\text{knee}}}{\overline{N_{ch}}(c_b)} \right)^{\alpha/2}, \quad (5)$$

and we assume for simplicity that r is independent of c_b . The three parameters $\sigma_{p_t}(0)$, α , and r are fitted to ATLAS data on the variance of p_t fluctuations [2, 13], in a range corresponding roughly to the 20% most central collisions. These data imply in particular that $[p_t]$ is strongly correlated with the density, which is reflected in the correlation coefficient r , which is close to 0.7.

A property of the two-dimensional Gaussian is that if one fixes one of the variables, e.g. N_{ch} , the distribution of the other variable, e.g. δp_t , is Gaussian (this property will be used below in order to evaluate the skewness and kurtosis). The distribution of δp_t at fixed N_{ch} and c_b is

defined by

$$p(\delta p_t | N_{ch}, c_b) = \frac{p(\delta p_t, N_{ch} | c_b)}{p(N_{ch} | c_b)}. \quad (6)$$

The distribution of δp_t at fixed N_{ch} is then obtained by averaging over impact parameter:

$$\begin{aligned} p(\delta p_t | N_{ch}) &= \int_0^1 p(\delta p_t | N_{ch}, c_b) p(c_b | N_{ch}) dc_b \\ &= \frac{1}{p(N_{ch})} \int_0^1 p(\delta p_t, N_{ch} | c_b) dc_b, \end{aligned} \quad (7)$$

where we have used Eqs. (4) and (6) in going from the first to the second line. The distributions $p(\delta p_t | N_{ch})$ are displayed as dashed lines in Fig. 2 for selected values of N_{ch} near the knee. The full lines in this figure are obtained by setting the correlation coefficient to its maximum value $r = 1$, corresponding to the simplified model of Eq. (1).

Once the distribution of δp_t is known, one can evaluate its cumulants. We derive semi-analytic expressions of the cumulants by using the property that the distribution of δp_t is Gaussian for fixed c_b :

$$P(\delta p_t | N_{ch}, c_b) = \frac{1}{\sqrt{2\pi\kappa_2(c_b)}} \exp\left(-\frac{(\delta p_t - \kappa_1(c_b))^2}{2\kappa_2(c_b)}\right), \quad (8)$$

where we omit the dependence on N_{ch} in the right-hand side. $\kappa_1(c_b)$ and $\kappa_2(c_b)$ are the mean and the variance at fixed N_{ch} and c_b , given by [2]:

$$\begin{aligned} \kappa_1(c_b) &= r \frac{\sigma_{p_t}(c_b)}{\sigma_{N_{ch}}(c_b)} (N_{ch} - \overline{N_{ch}}(c_b)) \\ \kappa_2(c_b) &= (1 - r^2) \sigma_{p_t}^2(c_b). \end{aligned} \quad (9)$$

Note that in the limit $r \rightarrow 1$, the variance $\kappa_2(c_b)$ vanishes and $P(\delta p_t | N_{ch}, c_b)$ reduces to a Dirac peak $\delta(\delta p_t - \kappa_1(c_b))$, implying that δp_t is solely determined by N_{ch} and c_b .

The moment of order n is obtained by multiplying Eq. (8) with δp_t^n and integrating over δp_t . One thus obtains the following expressions for the first four moments:

$$\begin{aligned} \langle \delta p_t | c_b \rangle &= \kappa_1 \\ \langle \delta p_t^2 | c_b \rangle &= \kappa_1^2 + \kappa_2 \\ \langle \delta p_t^3 | c_b \rangle &= \kappa_1^3 + 3\kappa_2\kappa_1 \\ \langle \delta p_t^4 | c_b \rangle &= \kappa_1^4 + 6\kappa_2\kappa_1^2 + 3\kappa_2^2, \end{aligned} \quad (10)$$

where the dependence on c_b on the right-hand side is implicit. These moments must then be averaged over c_b , as in Eq. (7). The cumulants are finally obtained from the moments using standard inversion formulas. The first four cumulants are the mean, the variance, the skewness and the excess kurtosis [31]:

$$\begin{aligned} \langle \delta p_t \rangle &= \langle \kappa_1 \rangle \\ \text{Var}(p_t) &= (\langle \kappa_1^2 \rangle - \langle \kappa_1 \rangle^2) + \langle \kappa_2 \rangle \\ \text{Skew}(p_t) &= \langle \kappa_1^3 \rangle - 3\langle \kappa_1^2 \rangle \langle \kappa_1 \rangle + 2\langle \kappa_1 \rangle^3 \end{aligned}$$

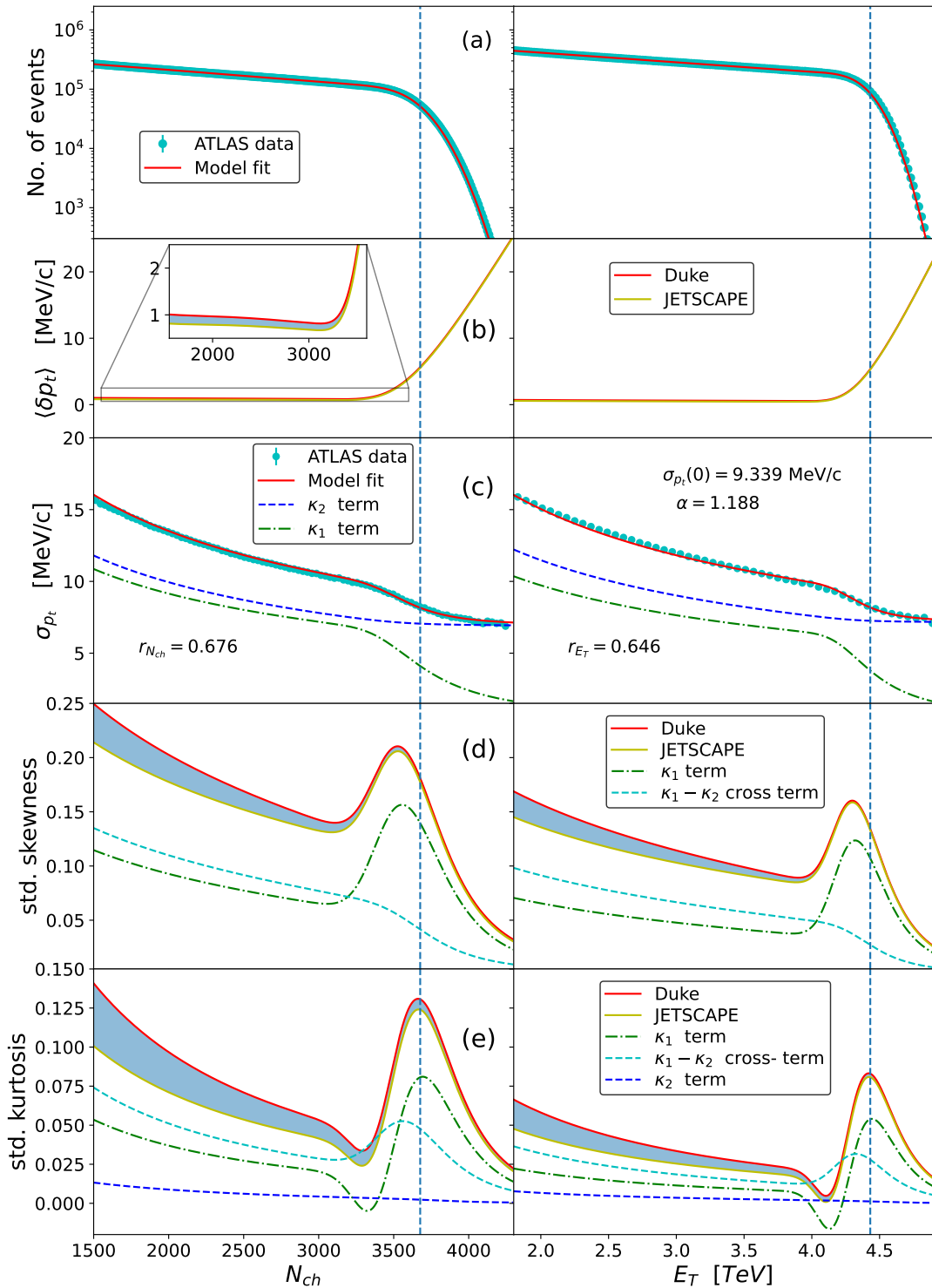


FIG. 3. (a) Histogram of the number of charged particles N_{ch} (left), measured in the inner detector of ATLAS, and of transverse energy E_T (right), measured in the forward and backward calorimeters. The vertical dashed line indicates the position of the knee. The next four panels display the first cumulants of the distribution of δp_t , calculated using Eq. (10), as a function of the centrality estimator. (b) Mean. (c) Standard deviation $\text{Var}(p_t)^{1/2}$. (d) Standardized skewness $\text{Skew}(p_t)/\text{Var}(p_t)^{3/2}$. (e) Standardized kurtosis $\text{Kurt}(p_t)/\text{Var}(p_t)^2$. The model is calibrated using ATLAS data for the standard deviation [13], shown as symbols in panel (c). In panels (b), (d) and (e), we display our predictions using the Duke and JETSCAPE parametrizations of the centrality dependence of $\sigma_{N_{ch}}$ (App. A). The difference between the two is negligible for the mean (see zoom in panel (b)) and the standard deviation (not shown), but is sizable for the skewness and kurtosis, where it is displayed as a shaded band. The contributions of the various terms in Eq. (11) are shown for the Duke parametrization only.

$$\begin{aligned} \text{Kurt}(p_t) = & +3(\langle\kappa_2\kappa_1\rangle - \langle\kappa_2\rangle\langle\kappa_1\rangle) \\ & \langle\kappa_1^4\rangle - 4\langle\kappa_1^3\rangle\langle\kappa_1\rangle + 6\langle\kappa_1^2\rangle\langle\kappa_1\rangle^2 - 3\langle\kappa_1\rangle^4 \\ & +6(\langle\kappa_2\kappa_1^2\rangle - \langle\kappa_2\rangle\langle\kappa_1^2\rangle) - 2\langle\kappa_2\kappa_1\rangle\langle\kappa_1\rangle + 2\langle\kappa_2\rangle\langle\kappa_1\rangle^2 \\ & +3(\langle\kappa_2^2\rangle - \langle\kappa_2\rangle^2). \end{aligned}$$

where angular brackets denote averages over c_b . One sees that κ_1 and κ_2 contribute separately to the variance. The term involving κ_1 is responsible for the sharp decrease of the variance around the knee, as shown in Ref. [2]. The skewness has terms involving κ_1 only, and a term proportional to the correlation between κ_1 and κ_2 . The kurtosis has one more term, which is proportional to the variance of κ_2 . The skewness and the kurtosis encode the non-Gaussian properties of the event-by-event fluctuations of $[p_t]$. In our model, which assumes Gaussian fluctuations at fixed impact parameter, all non-Gaussianities originate from impact parameter fluctuations. If the impact parameter does not fluctuate, each line in Eq. (11) is identically zero.

Our quantitative predictions are displayed in panels (b), (d) and (e) of Fig. 3. The increase of the mean, displayed in panel (b), has already been discussed in the literature [2, 32, 33]. The new results of this paper are the skewness and the kurtosis, which both display sharp variations around the knee. We predict an increase of the skewness below the knee, which has already been reported by the ALICE collaboration [34]. This increase is followed by a fast decrease. The kurtosis has first a minimum, followed by a maximum roughly at the knee. These structures come from the terms involving κ_1 , and are inherited from the truncated Gaussian. The cumulants of the truncated Gaussian (4) can be calculated analytically. The maximum of the skewness occurs at $N_{ch} \simeq N_{\text{knee}} - \sigma_{N_{ch}} \simeq 3510$. The kurtosis has a minimum at $N_{ch} \simeq N_{\text{knee}} - 2\sigma_{N_{ch}} \simeq 3340$, followed by a maximum at $N_{ch} \simeq N_{\text{knee}} \simeq 3680$. This corresponds to the structure seen in our numerical results.

One sees that our predictions depend little on which scenario (Duke or JETSCAPE) one chooses for the centrality dependence of multiplicity fluctuations. The main limitation of our model is that we have assumed a Gaussian distribution of $[p_t]$ at fixed N_{ch} and b . Since $[p_t]$ is a positive quantity, one expects its distribution to have a positive skewness κ_3 and a positive excess kurtosis κ_4 . This will give additional positive contributions to $\text{Skew}(p_t)$ and $\text{Kurt}(p_t)$ in Eq. (11), of the form $\langle\kappa_3\rangle$ and $\langle\kappa_4\rangle$, so that our predictions should be considered a lower bound, both for the skewness and for the kurtosis. Predicting quantitatively the value of this additional term is difficult and would require high-statistics hydrodynamic simulation. We can however safely state that the additional contributions should have a smooth dependence on N_{ch} , and will typically result in a positive offset from our prediction. The sharp *variations* of the skewness and kurtosis around the knee in Fig. 3 (c) and (d) are robust, quantitative predictions.

Finally, the ATLAS collaboration also carries out analyses by estimating the centrality using the transverse energy E_T deposited in two calorimeters symmetrically

with respect to the collision point, at smaller angles with respect to the beam than the inner detector. The whole analysis can be repeated by replacing N_{ch} with E_T everywhere, as shown in the right panel of Fig. 3. It turns out that E_T is a better centrality estimator than N_{ch} , which results in smaller impact parameter fluctuations [24, 35]. Since, in our model, all the non-Gaussianities originate from impact parameter fluctuations, one expects that both the skewness and the kurtosis are smaller if the centrality is determined as a function of E_T , which is exactly seen in our predictions. Experimental verification of these predictions will be crucial in assessing the importance of impact parameter fluctuations.

ACKNOWLEDGMENTS

We thank Somadutta Bhatta and Jiangyong Jia for suggesting us to publish quantitative predictions for the skewness. We thank the Institute for Nuclear Theory at the University of Washington for hosting the program “Intersection of nuclear structure and high-energy nuclear collisions” during which this work was initiated. R. S. is supported by the Polish grant NAWA PRELUDIUM BIS: PPN/STA/2021/1/00040/U/00001 and the NCN grant PRELUDIUM BIS: 2019/35/O/ST2/00357. M. L. thanks the São Paulo Research Foundation (FAPESP) for support under grants 2021/08465-9, 2018/24720-6, and 2017/05685-2, as well as the support of the Brazilian National Council for Scientific and Technological Development (CNPq). We acknowledge support from the “Emilie du Châtelet” visitor programme and from the GLUODYNAMICS project funded by the “P2IO LabEx (ANR-10-LABX-0038)” in the framework “Investissements d’Avenir” (ANR-11-IDEX-0003-01) managed by the Agence Nationale de la Recherche (ANR).

Appendix A: Centrality dependence of multiplicity fluctuations

The probability distribution of the multiplicity at fixed impact parameter b is expected to be approximately Gaussian [23] and can be characterized by its mean $\overline{N_{ch}}$ and standard deviation $\sigma_{N_{ch}}$, which both depend on b . The mean can be reconstructed using the simple following rule. If a fraction c_b of events have a multiplicity larger than N , then $N \simeq \overline{N_{ch}}(c_b)$ [39]. This simple rule, which is applied to ATLAS data in Fig. 4 (a), works well except for multiplicities around and above the knee.

On the other hand, the centrality dependence of $\sigma_{N_{ch}}$ is not known, and we use state-of-the art hydrodynamic calculations by the Duke group [28] and by the JETSCAPE collaboration [29] to evaluate it. However, we want to avoid running massive hydrodynamic calculations, and we therefore estimate the multiplicity fluctuations from the initial conditions of these calculations. We assume that for every collision event, the multiplicity is propor-

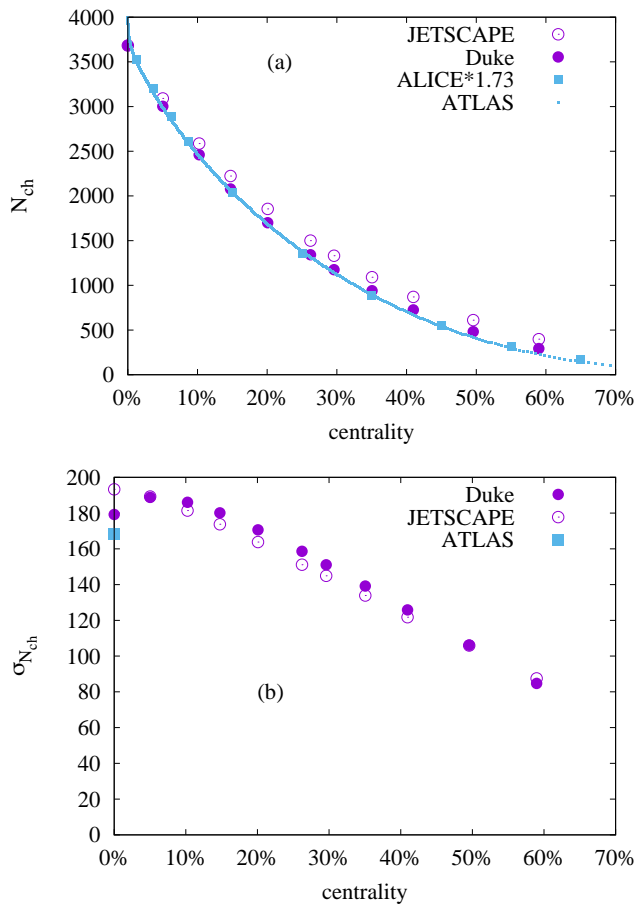


FIG. 4. (a) Variation of charged multiplicity N_{ch} with centrality in Pb+Pb collisions at $\sqrt{s_{NN}} = 5.02$ TeV measured by ATLAS [13] and ALICE [36]. For ATLAS, the centrality is defined from the cumulative distribution of N_{ch} and then divided by a calibration factor 1.153 [37], which corrects for the fact that for the largest centrality fractions, some of the recorded events are fake. The ALICE results have been rescaled by a factor 1.73 to correct for the different acceptance and efficiency of the detector. The circles display the centrality dependence of the mean initial energy for the T_{RENT}o parametrizations used by the Duke [28] and JETSCAPE analyses [29]. The centrality is defined as $\pi b^2/\sigma_{Pb}$, where $\sigma_{Pb} = 767$ fm² is the total inelastic cross section. (b) Variation of the standard deviation of N_{ch} with centrality.

tional to the initial energy. Both Duke and JETSCAPE analyses employ the T_{RENT}o parametrization [38] for the initial energy density, but with slightly different values of the parameters. We run these T_{RENT}o initial conditions for several fixed values of b (specifically, $b = 0, 3.5, 5, 6, 7, 8, 8.5, 9.25, 10, 10.5, 11, 11.5, 12$ fm). For each b , we generate 10^5 events with both Duke and JETSCAPE parameters, and we compute the initial energy of each event. We rescale this energy by a constant factor so

that it matches the ATLAS result for the charged multiplicity at $b = 0$ [2]. The variation of the mean N_{ch} with centrality is displayed in Fig. 4 (a). Experimental data are also shown. One sees that ALICE and ATLAS data are in excellent agreement once properly rescaled. The calculation using the Duke parametrization agrees very well with experiment. Agreement is not quite as good, but still reasonable, for the JETSCAPE parametrization.

We then calculate the standard deviation of N_{ch} , $\sigma_{N_{ch}}$, for each value of b . Results are displayed in Fig. 4 (b). The standard deviation can only be measured at $b = 0$ [35] from the tail of the distribution of N_{ch} , therefore, there is only one data point on this plot. One sees that both model calculations are in reasonable agreement with this data point, but slightly overestimate it.

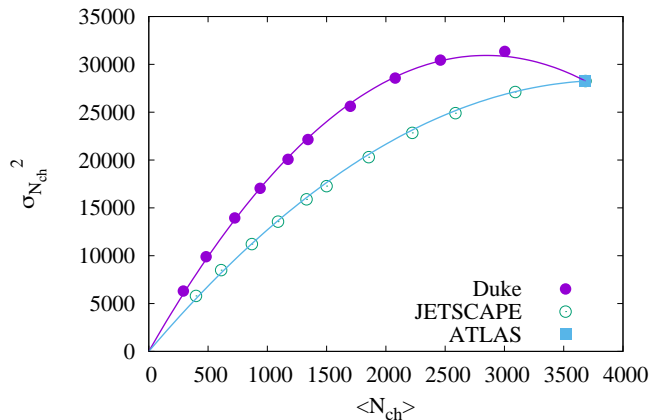


FIG. 5. Parametric plot of the mean and variance of N_{ch} as a function of b . Both models have been calibrated in such a way that they match data at $b = 0$. Solid lines are fits using $y = \gamma x + (1 - \gamma)x^2$, where $y \equiv \sigma_{N_{ch}}^2(b)/\sigma_{N_{ch}}^2(0)$ and $x \equiv \langle N_{ch} \rangle(b)/\langle N_{ch} \rangle(0)$, with $\gamma = 2.83$ (Duke) and $\gamma = 1.90$ (JETSCAPE). The calculation in Ref. [2] was done with $\gamma = 1$ (variance proportional to mean).

We use model calculations only to predict the b -dependence of $\sigma_{N_{ch}}$, not the value at $b = 0$ which is measured precisely. We therefore rescale $\sigma_{N_{ch}}$ from the model calculation by a constant factor so that it matches the experimental value at $b = 0$. The resulting predictions for $b > 0$ are displayed in Fig. 5. We plot the variance $\sigma_{N_{ch}}^2$ as a function of the mean. If N_{ch} is the sum of k identical, uncorrelated distributions, where k depends on b , both the mean and the variance are proportional to k , therefore, they are proportional to one another. This behavior is only observed for large values of b . Both model calculations predict that the variance increases more slowly as b decreases. The Duke calculation even predicts that it decreases for the smallest values of b . The two solid lines, which are polynomial fits to our calculations, are used as two limiting cases which define the error bands in Fig. 3.

- [1] U. Heinz and R. Snellings, *Ann. Rev. Nucl. Part. Sci.* **63**, 123-151 (2013) doi:10.1146/annurev-nucl-102212-170540 [arXiv:1301.2826 [nucl-th]].
- [2] R. Samanta, S. Bhatta, J. Jia, M. Luzum and J. Y. Ollitrault, [arXiv:2303.15323 [nucl-th]].
- [3] H. Appelshäuser *et al.* [NA49], *Phys. Lett. B* **459**, 679-686 (1999) doi:10.1016/S0370-2693(99)00673-5 [arXiv:hep-ex/9904014 [hep-ex]].
- [4] D. Adamova *et al.* [CERES], *Nucl. Phys. A* **727**, 97-119 (2003) doi:10.1016/j.nuclphysa.2003.07.018 [arXiv:nucl-ex/0305002 [nucl-ex]].
- [5] J. Adams *et al.* [STAR], *Phys. Rev. C* **71**, 064906 (2005) doi:10.1103/PhysRevC.71.064906 [arXiv:nucl-ex/0308033 [nucl-ex]].
- [6] S. S. Adler *et al.* [PHENIX], *Phys. Rev. Lett.* **93**, 092301 (2004) doi:10.1103/PhysRevLett.93.092301 [arXiv:nucl-ex/0310005 [nucl-ex]].
- [7] J. Adams *et al.* [STAR], *Phys. Rev. C* **72**, 044902 (2005) doi:10.1103/PhysRevC.72.044902 [arXiv:nucl-ex/0504031 [nucl-ex]].
- [8] B. B. Abelev *et al.* [ALICE], *Eur. Phys. J. C* **74**, no.10, 3077 (2014) doi:10.1140/epjc/s10052-014-3077-y [arXiv:1407.5530 [nucl-ex]].
- [9] W. Broniowski, M. Chojnacki and L. Obara, *Phys. Rev. C* **80**, 051902 (2009) doi:10.1103/PhysRevC.80.051902 [arXiv:0907.3216 [nucl-th]].
- [10] J. E. Bernhard, J. S. Moreland and S. A. Bass, *Nature Phys.* **15**, no.11, 1113-1117 (2019) doi:10.1038/s41567-019-0611-8
- [11] D. Everett *et al.* [JETSCAPE], *Phys. Rev. Lett.* **126**, no.24, 242301 (2021) doi:10.1103/PhysRevLett.126.242301 [arXiv:2010.03928 [hep-ph]].
- [12] G. Nijs, W. van der Schee, U. Gürsoy and R. Snellings, *Phys. Rev. Lett.* **126**, no.20, 202301 (2021) doi:10.1103/PhysRevLett.126.202301 [arXiv:2010.15130 [nucl-th]].
- [13] G. Aad *et al.* [ATLAS], *Phys. Rev. C* **107**, no.5, 054910 (2023) doi:10.1103/PhysRevC.107.054910 [arXiv:2205.00039 [nucl-ex]].
- [14] M. Luzum and J. Y. Ollitrault, *Nucl. Phys. A* **904-905**, 377c-380c (2013) doi:10.1016/j.nuclphysa.2013.02.028 [arXiv:1210.6010 [nucl-th]].
- [15] S. Chatrchyan *et al.* [CMS], *JHEP* **02**, 088 (2014) doi:10.1007/JHEP02(2014)088 [arXiv:1312.1845 [nucl-ex]].
- [16] S. Plumari, G. L. Guardo, F. Scardina and V. Greco, *Phys. Rev. C* **92**, no.5, 054902 (2015) doi:10.1103/PhysRevC.92.054902 [arXiv:1507.05540 [hep-ph]].
- [17] C. Shen, Z. Qiu and U. Heinz, *Phys. Rev. C* **92**, no.1, 014901 (2015) doi:10.1103/PhysRevC.92.014901 [arXiv:1502.04636 [nucl-th]].
- [18] P. Carzon, S. Rao, M. Luzum, M. Sievert and J. Noronha-Hostler, *Phys. Rev. C* **102**, no.5, 054905 (2020) doi:10.1103/PhysRevC.102.054905 [arXiv:2007.00780 [nucl-th]].
- [19] L. M. Liu, C. J. Zhang, J. Zhou, J. Xu, J. Jia and G. X. Peng, *Phys. Lett. B* **834**, 137441 (2022) doi:10.1016/j.physletb.2022.137441 [arXiv:2203.09924 [nucl-th]].
- [20] A. V. Giannini *et al.* [ExTrEMe], *Phys. Rev. C* **107**, no.4, 044907 (2023) doi:10.1103/PhysRevC.107.044907 [arXiv:2203.17011 [nucl-th]].
- [21] K. Kuroki, A. Sakai, K. Murase and T. Hirano, *Phys. Lett. B* **842**, 137958 (2023) doi:10.1016/j.physletb.2023.137958 [arXiv:2305.01977 [nucl-th]].
- [22] G. Giacalone, F. G. Gardim, J. Noronha-Hostler and J. Y. Ollitrault, *Phys. Rev. C* **103**, no.2, 024910 (2021) doi:10.1103/PhysRevC.103.024910 [arXiv:2004.09799 [nucl-th]].
- [23] S. J. Das, G. Giacalone, P. A. Monard and J. Y. Ollitrault, *Phys. Rev. C* **97**, no.1, 014905 (2018) doi:10.1103/PhysRevC.97.014905 [arXiv:1708.00081 [nucl-th]].
- [24] M. Pepin, P. Christiansen, S. Munier and J. Y. Ollitrault, *Phys. Rev. C* **107**, no.2, 024902 (2023) doi:10.1103/PhysRevC.107.024902 [arXiv:2208.12175 [nucl-th]].
- [25] B. Alver *et al.* [PHOBOS], *Phys. Rev. Lett.* **98**, 242302 (2007) doi:10.1103/PhysRevLett.98.242302 [arXiv:nucl-ex/0610037 [nucl-ex]].
- [26] M. L. Miller, K. Reygers, S. J. Sanders and P. Steinberg, *Ann. Rev. Nucl. Part. Sci.* **57**, 205-243 (2007) doi:10.1146/annurev.nucl.57.090506.123020 [arXiv:nucl-ex/0701025 [nucl-ex]].
- [27] F. Gelis, E. Iancu, J. Jalilian-Marian and R. Venugopalan, *Ann. Rev. Nucl. Part. Sci.* **60**, 463-489 (2010) doi:10.1146/annurev.nucl.010909.083629 [arXiv:1002.0333 [hep-ph]].
- [28] J. S. Moreland, J. E. Bernhard and S. A. Bass, *Phys. Rev. C* **101**, no.2, 024911 (2020) doi:10.1103/PhysRevC.101.024911 [arXiv:1808.02106 [nucl-th]].
- [29] D. Everett *et al.* [JETSCAPE], *Phys. Rev. C* **103**, no.5, 054904 (2021) doi:10.1103/PhysRevC.103.054904 [arXiv:2011.01430 [hep-ph]].
- [30] S. Acharya *et al.* [ALICE], *Phys. Lett. B* **788**, 166-179 (2019) doi:10.1016/j.physletb.2018.10.052 [arXiv:1805.04399 [nucl-ex]].
- [31] S. Bhatta, C. Zhang and J. Jia, *Phys. Rev. C* **105**, no.2, 024904 (2022) doi:10.1103/PhysRevC.105.024904 [arXiv:2112.03397 [nucl-th]].
- [32] F. G. Gardim, G. Giacalone and J. Y. Ollitrault, *Phys. Lett. B* **809**, 135749 (2020) doi:10.1016/j.physletb.2020.135749 [arXiv:1909.11609 [nucl-th]].
- [33] G. Nijs and W. van der Schee, *Phys. Rev. C* **106**, no.4, 044903 (2022) doi:10.1103/PhysRevC.106.044903 [arXiv:2110.13153 [nucl-th]].
- [34] S. Saha [ALICE], *PoS ICHEP2022*, 1157 (2022) doi:10.22323/1.414.1157
- [35] K. V. Yusefina, A. Kotibhaskar, R. Bhalariao and J. Y. Ollitrault, *Phys. Rev. C* **105**, no.1, 014907 (2022) doi:10.1103/PhysRevC.105.014907 [arXiv:2108.03471 [nucl-th]].
- [36] J. Adam *et al.* [ALICE], *Phys. Rev. Lett.* **116**, no.22, 222302 (2016) doi:10.1103/PhysRevLett.116.222302 [arXiv:1512.06104 [nucl-ex]].
- [37] M. Aaboud *et al.* [ATLAS], *Eur. Phys. J. C* **78**, no.12, 997 (2018) doi:10.1140/epjc/s10052-018-6468-7

- [arXiv:1808.03951 [nucl-ex]].
- [38] J. S. Moreland, J. E. Bernhard and S. A. Bass, Phys. Rev. C **92**, no.1, 011901 (2015) doi:10.1103/PhysRevC.92.011901 [arXiv:1412.4708 [nucl-th]].
- [39] W. Broniowski and W. Florkowski, Phys. Rev. C **65**, 024905 (2002) doi:10.1103/PhysRevC.65.024905 [arXiv:nucl-th/0110020 [nucl-th]].